# Supplementary Information

# Degradation Mechanism of Hybrid Tin-Based Perovskite Solar Cells and the Critical Role of Tin (IV) Iodide

Luis Lanzetta[1], Thomas Webb[1,†], Nourdine Zibouche[2,†], Xinxing Liang[1], Dong Ding[1], Ganghong Min[1], Robert J. E. Westbrook[1], Benedetta Gaggio, Thomas J. Macdonald[1], M. Saiful Islam[2]*, Saif A. Haque[1]*.

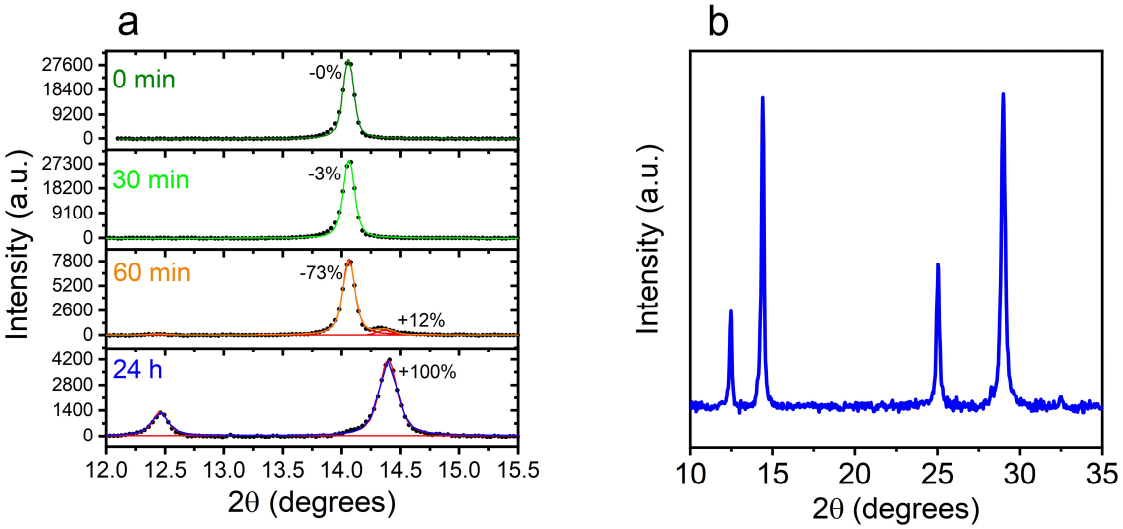
[1]Department of Chemistry and Centre for Processable Electronics, Molecular Sciences Research Hub, Imperial College London, London W12 0BZ, UK

[2]Department of Chemistry, University of Bath, Bath BA2 7AY, UK

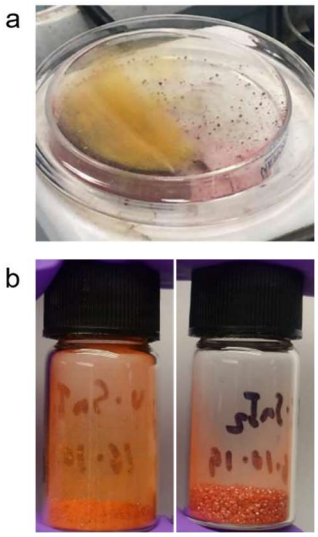
[†]These authors contributed equally to this work

*Corresponding authors: m.s.islam@bath.ac.uk; s.a.haque@imperial.ac.uk

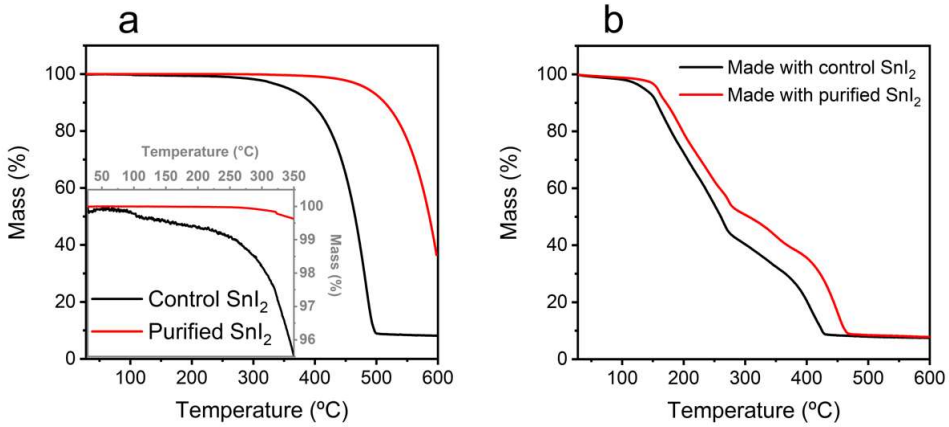
**Supplementary Note 1:** $I_2$-degraded perovskite films ($SnI_4$-rich) exposed to ambient air for further 10 minutes result in toluene extractions showing stronger absorption at ~300 and ~500 nm relative to samples exposed to $I_2$ vapour only (Figure 4c); this observation being consistent with the rapid evolution (< 10 min) of $SnI_4$ to $I_2$ via Reactions 3 and 4.



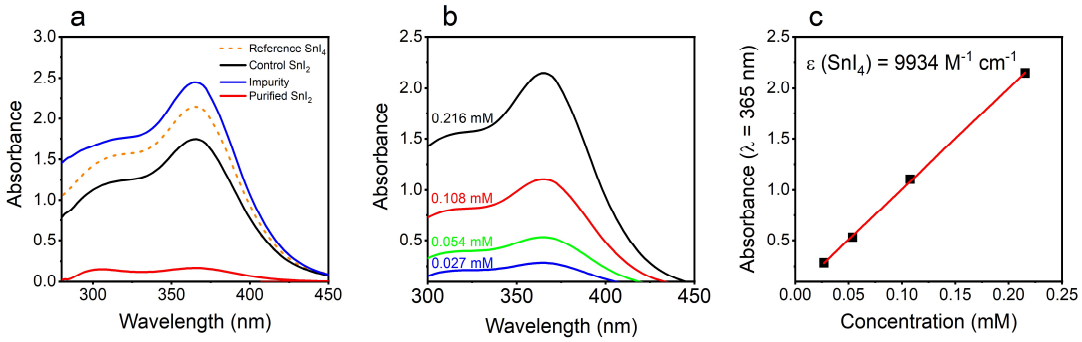

**Supplementary Figure 1. a.** Powder X-Ray diffraction (XRD) patterns of a $(PEA)_{0.2}(FA)_{0.8}SnI_3$ film degraded in ambient air for 0 min, 30 min, 60 min and 24 h (black dots). Patterns are deconvoluted into Voigt peak functions (colour lines: cumulative fittings; red lines: single peak functions) to estimate the percentage of perovskite signal loss (relatively to signal at 0 min) and double perovskite signal gain (normalised to signal at 24 h). **b.** Powder XRD pattern of a $(PEA)_{0.2}(FA)_{0.8}SnI_3$ thin film degraded in ambient air for 24 h. Peaks are assigned to the vacancy-ordered double perovskite derivative $FA_2SnI_6$. We note that the absence of $SnO_2$ reflections is likely owed to the highly disordered/amorphous character of this degradation product, in agreement with previous work.[1]



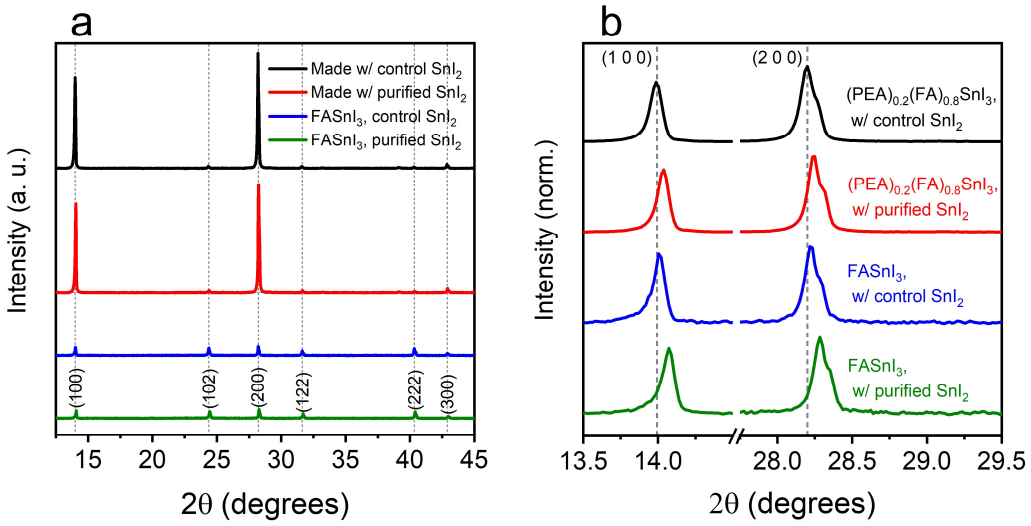

**Supplementary Figure 2.** $SnI_2$ purification heat treatment. **a.** Image of the treatment setup: commercial $SnI_2$ is placed inside a covered Petri dish and heated at 250ºC for 1h in a $N_2$-filled glovebox. $SnI_4$ is removed from $SnI_2$ via sublimation and deposited on the inner side of the lid. The purification of $SnI_2$ via sublimation of $SnI_4$ exploits the much higher volatility of the latter, being a molecular solid in contrast with ionic $SnI_2$. **b.** Image of vials containing $SnI_2$ before (left) and after (right) the purification treatment.



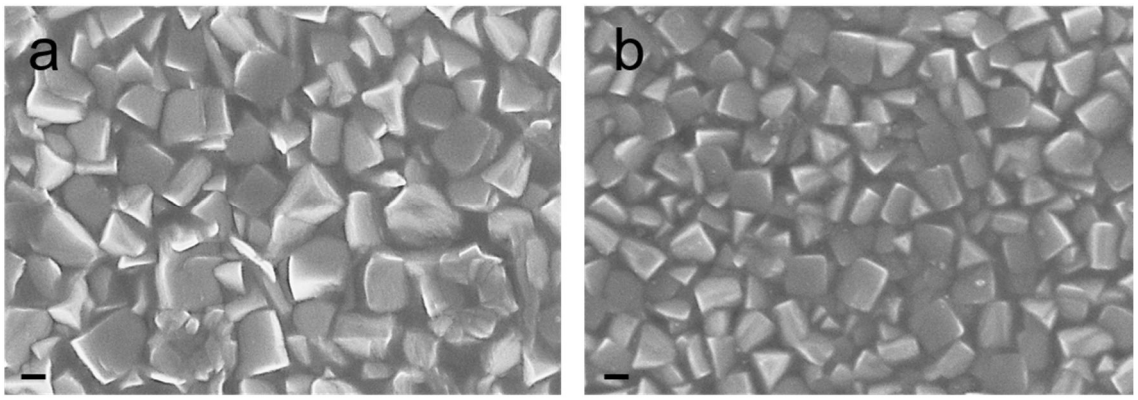

**Supplementary Figure 3.** Thermogravimetric analysis (TGA) of $SnI_2$ precursors and $(PEA)_{0.2}(FA)_{0.8}SnI_3$ perovskite registered under $N_2$. **a.** TGA curves of control $SnI_2$ and purified $SnI_2$. Inset: magnification of main graph at 40-350ºC temperature range. The initial decrease in mass in control $SnI_2$ is 0.5% approximately and starts at relatively low temperatures (~100ºC), while purified $SnI_2$ only exhibits a mass drop from ~300ºC attributed to $SnI_2$ evaporation. **b.** TGA curves of $(PEA)_{0.2}(FA)_{0.8}SnI_3$ perovskite made with control $SnI_2$ and purified $SnI_2$. The curves shows two distinctive mass losses corresponding to i) the evaporation of the organic salts and ii) the sublimation of $SnI_2$ at higher temperatures, in good agreement with previous reports.[2] We note that perovskite made with control $SnI_2$ shows mass losses at lower temperatures throughout the scan, being this difference more accentuated in the second mass loss step in consistence with $SnI_2$ richer in more volatile $Sn^{4+}$ impurities.



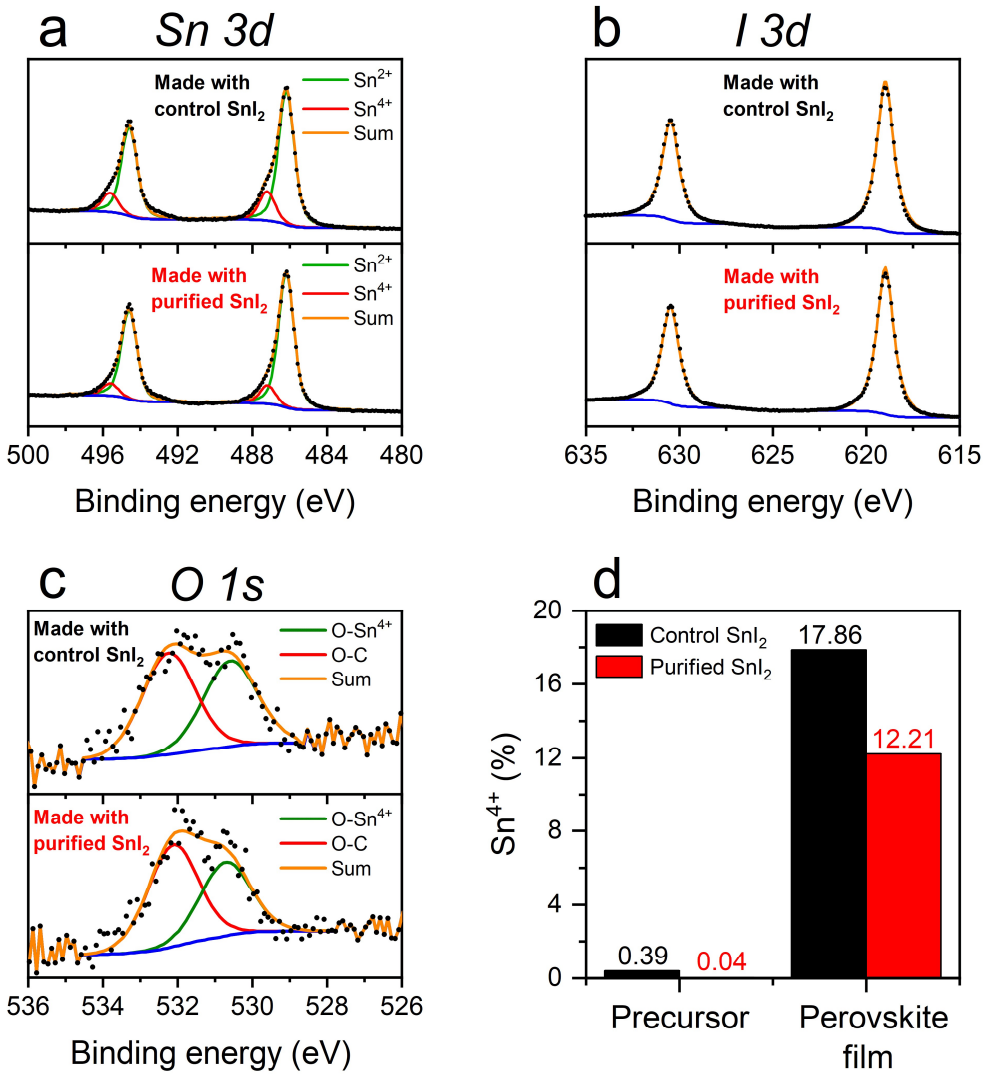

**Supplementary Figure 4. a.** UV-Visible absorbance spectra of impurities dissolved in ultradry toluene ($SnI_4$ is highly soluble in non-polar solvents like toluene, unlike $SnI_2$) and extracted from 0.05 g control $SnI_2$ (red; 3 mL toluene used), 0.05 g purified $SnI_2$ (black; 3 mL toluene used) and the solidified phase eliminated from control $SnI_2$ via sublimation (blue). These absorption spectra match the one recorded for a 0.216 mM $SnI_4$ reference solution in toluene (dashed orange line), allowing to identify the impurity as $SnI_4$. **b.** UV-Visible absorbance spectra of reference $SnI_4$ solutions in toluene at different concentrations. **c.** Absorbance ($\lambda$ = 365 nm) vs concentration plot obtained from data in Supplementary Figure 4b and its linear fitting ($\varepsilon(SnI_4)$ = 9934 $M^{-1}$ $cm^{-1}$). We obtain the mass percentage of $SnI_4$ in the precursor before and after the heat treatment by applying the Beer-Lambert Law ($A = \varepsilon cl$; $l$ = 1 cm) to calculate the concentration of $SnI_4$ in the toluene extractions (Supplementary Figure 4a) from their absorbance at 365 nm. Control $SnI_2$ contains 0.65% $SnI_4$ in mass, while only 0.06% $SnI_4$ is found in purified $SnI_2$.




**Supplementary Figure 5. a.** Powder XRD patterns of glass/$(PEA)_{0.2}(FA)_{0.8}SnI_3$ and $FASnI_3$ thin films made with control/purified $SnI_2$. The indexed diffraction peaks reveal that perovskites possess an orthorhombic crystal structure (Amm2 space group), consistent with the α-phase of $FASnI_3$.[3] In contrast with archetypal 3D $FASnI_3$ film, peaks in patterns of $(PEA)_{0.2}(FA)_{0.8}SnI_3$ films provide much higher diffraction intensity, indicating that the addition of PEAI increases the crystallinity of the final perovskite. Furthermore, this also causes (h00) reflections in the diffractogram to clearly become more prominent (particularly (100) and (200)), which suggests that perovskite crystals preferentially grow with their {h00} planes oriented parallel to the substrate.[4,5] Diffraction patterns of $(PEA)_{0.2}(FA)_{0.8}SnI_3$ do not present significant changes when the control or purified $SnI_2$ is employed, confirming that the perovskite crystalline structure is not altered as a consequence of the purification of the precursor. **b.** Magnified X-ray diffraction patterns of (100) and (200) main reflections acquired from $(PEA)_{0.2}(FA)_{0.8}SnI_3$ and $FASnI_3$ films made with control/purified $SnI_2$. Peaks from perovskites made with purified $SnI_2$ are shifted to higher diffraction angles, indicative of smaller lattice parameters. We suggest that reducing the incorporation of $Sn^{4+}$ into perovskite may result in less $Sn^{2+}/I^-$ vacancies in the lattice and therefore more compact unit cells.



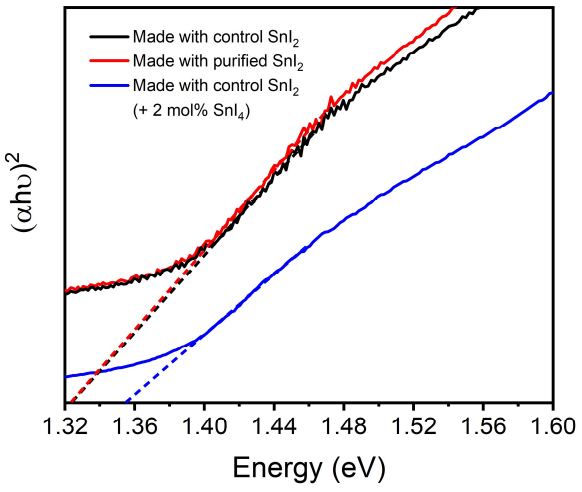

**Supplementary Figure 6.** Top-view Scanning Electron Microscopy (SEM) images of $(PEA)_{0.2}(FA)_{0.8}SnI_3$ perovskite thin films deposited on PEDOT:PSS. Scale bar: 200 nm. **a.** Film made with control $SnI_2$. **b.** Film made with purified $SnI_2$. SEM images reveal submicron-sized quasi-cubic perovskite grains, being these slightly smaller in samples made with purified $SnI_2$.



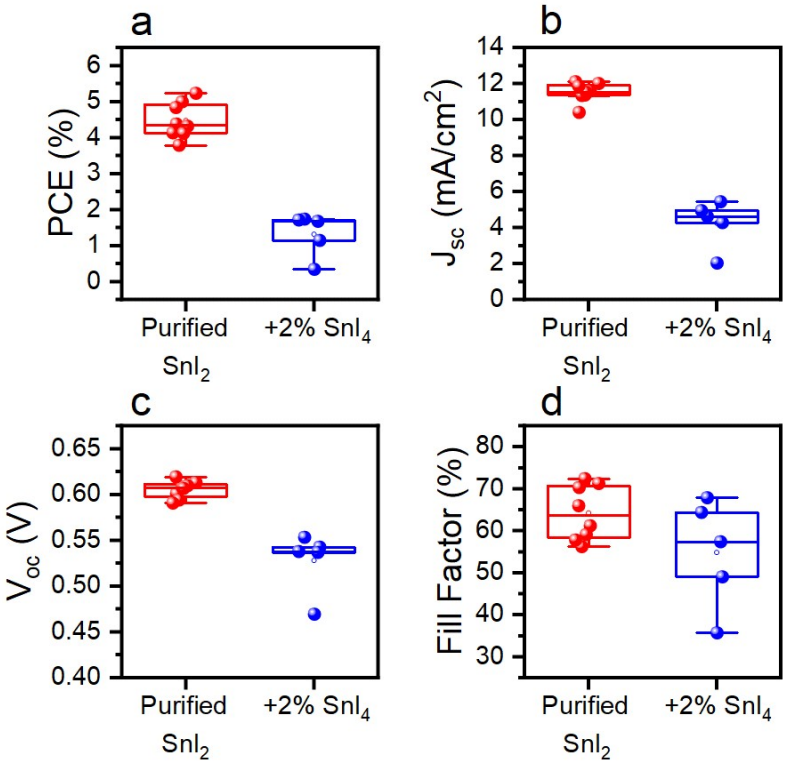

**Supplementary Figure 7.** Surface X-Ray Photoelectron Spectroscopy (XPS) spectra of ITO/PEDOT:PSS/$(PEA)_{0.2}(FA)_{0.8}SnI_3$ films made with control/purified $SnI_2$ and their deconvolution. Further details on species assignation are provided in Supplementary Table 1. **a.** Sn $3d_{5/2}$ and Sn $3d_{3/2}$ XPS peaks of perovskite films. We deconvolute the XPS spectra into two regions assigned to $Sn^{2+}$ in perovskite (~486.18 eV, ~494.59 eV) and a combination of $Sn^{4+}$ states ($SnO_2$ + perovskite $Sn^{4+}$ centres; ~487.21 eV, ~495.62 eV). The total contribution (peak area percentage) of the $Sn^{4+}$ component decreases from 17.86% to 12.21% when using purified $SnI_2$ instead of control $SnI_2$, verifying that using $Sn^{4+}$-poorer precursors leads to fewer $Sn^{4+}$ states in the perovskite. **b.** I $3d_{5/2}$ and I $3d_{3/2}$ XPS peaks of perovskite films. Spectra are fitted to a single component assigned to iodide in the perovskite structure. **c.** O 1*s* spectra of perovskite films. Spectra are deconvoluted into two regions assigned to $SnO_2$ (O-$Sn^{4+}$; ~530.66 eV) and adventitious organic contaminants (O-C; 532.18 eV). **d.** $Sn^{4+}$ content (i.e. percentage of Sn atoms with oxidation state IV) in $SnI_2$ precursors (measured with UV-Visible spectroscopy; Beer-Lambert Law) and $(PEA)_{0.2}(FA)_{0.8}SnI_3$ films (measured with XPS). We find that the percentage of $Sn^{4+}$ states in the perovskite films is considerably higher compared to the values obtained in the $SnI_2$ precursors, suggesting that $Sn^{2+}$ undergoes oxidation in the intermediate steps of film processing/storage prior to measurement.

| Precursor used | | $Sn^{2+}$ | $Sn^{4+}$ | $I^-$ | O-$Sn^{4+}$ |
|---|---|---|---|---|---|
| Control $SnI_2$ | Area/(RSF*T*MFP) | 2612.310 | 567.974 | 8058.600 | 356.603 |
| | Atomic ratio vs $Sn^{2+}$ | 1.000 | 0.217 | 3.085 | 0.137 |
| Purified $SnI_2$ | Area/(RSF*T*MFP) | 2747.850 | 382.075 | 8648.270 | 367.869 |
| | Atomic ratio vs $Sn^{2+}$ | 1.000 | 0.139 | 3.147 | 0.134 |

**Supplementary Table 1.** Corrected areas and atomic ratios (vs $Sn^{2+}$) obtained from XPS components in Supplementary Figures 7a, 7b and 7c. We observe that the O-$Sn^{4+}$ ratios are comparable in both samples (0.137 vs 0.134), indicating a similar $SnO_2$ concentration at the surface in both cases. Assuming 1:2 stoichiometry, the $Sn^{4+}$ ratios corresponding to $SnO_2$ are estimated as 0.069 and 0.067 for films made with control and purified $SnI_2$, respectively. The remaining $Sn^{4+}$ states (control $SnI_2$: 0.217-0.069 = 0.148; purified $SnI_2$: 0.139-0.067 = 0.072) are assigned to $Sn^{4+}$ centres in the perovskite structure. Hence, the main effect of using purified precursors is a decrease in $Sn^{4+}$ centres in the perovskite. We consider any major contribution from $SnI_4$ or $FA_2SnI_6$ to the $Sn^{4+}$ component unlikely due to i) $SnI_4$ being highly volatile and rapidly evaporating from the film at vacuum levels used in XPS ($10^{-6}$ mbar or lower) and ii) the $I^-$ ratios being close to 3 in consistence with the perovskite stoichiometry ($I^-$ ratios expected to be significantly higher if $Sn^{4+}$ components were caused by $SnI_4$ or $FA_2SnI_6$).



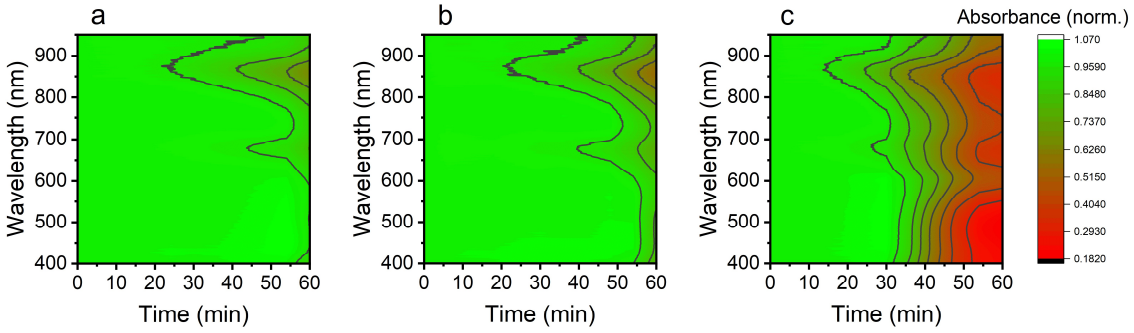

**Supplementary Figure 8.** Tauc plots of $(PEA)_{0.2}(FA)_{0.8}SnI_3$ perovskite films made with control $SnI_2$ (black line), purified $SnI_2$ (red line) and control $SnI_2$ + 2 mol% $SnI_4$. The resulting bandgaps are 1.32 eV, 1.32 eV and 1.35 eV, respectively.



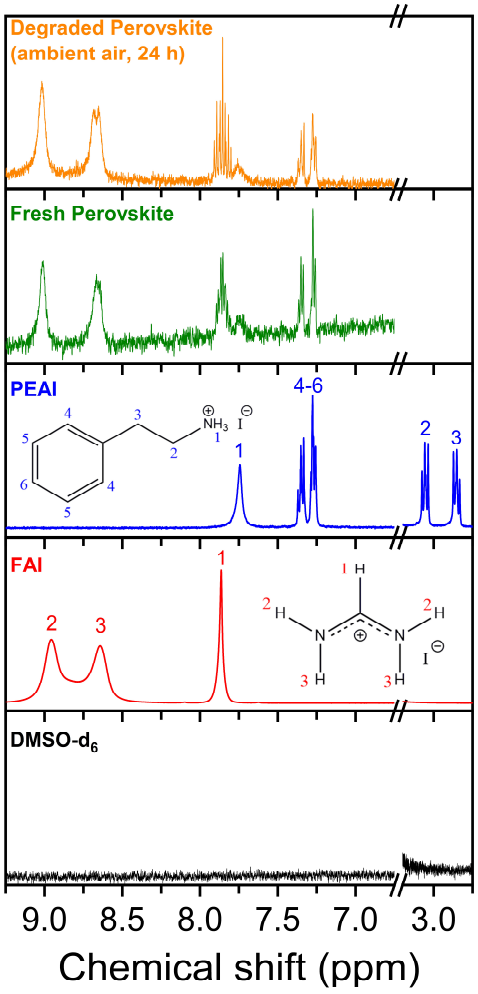

**Supplementary Figure 9. a.** PCE, **b.** $J_{sc}$, **c.** $V_{oc}$ and **d.** Fill Factor statistics of cells made with purified $SnI_2$ (8 devices) and with control $SnI_2$ + 2 mol% $SnI_4$ (5 devices). Box range: 25th-75th percentiles; centre line: median; whiskers: 1.5x interquartile range.

| Precursor Type | PCE(%) | $V_{oc}$ (V) | $J_{sc}$ | FF (%) |
|---|---|---|---|---|
| **Purified $SnI_2$** | 4.47 ± 0.50 (5.23) | 0.61 ± 0.01 (0.61) | 11.52 ± 0.54 (12.00) | 64.27 ± 6.50 (71.19) |
| **Control $SnI_2$ (+ 2% $SnI_4$)** | 1.32 ± 0.60 (1.73) | 0.53 ± 0.03 (0.55) | 4.26 ± 1.31 (4.61) | 54.89 ± 12.94 (67.90) |

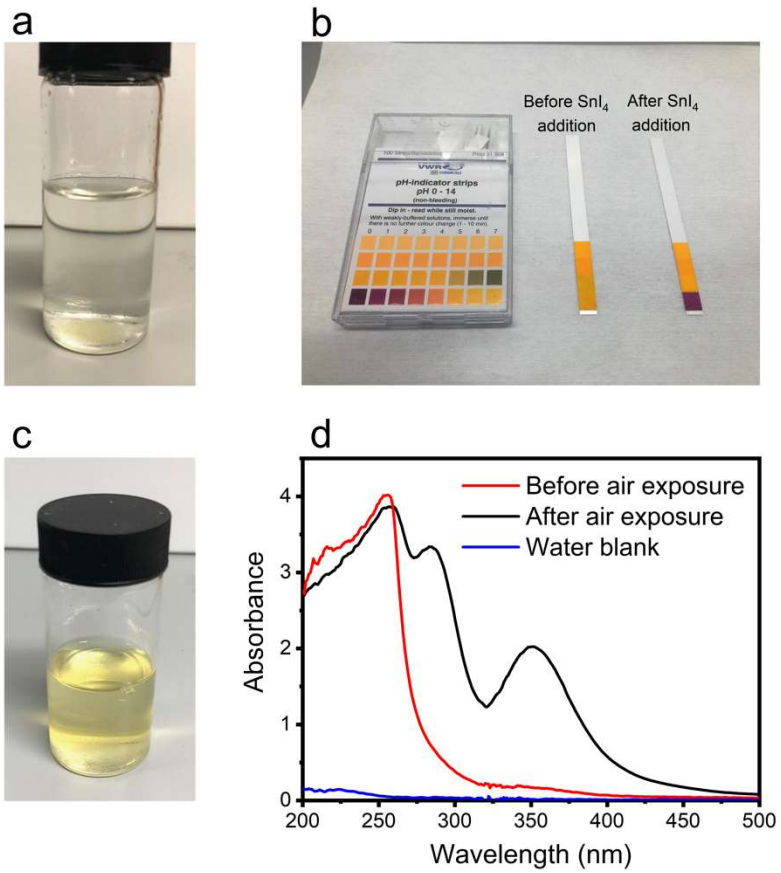
**Supplementary Table 2.** Mean values for solar cell PCE, $J_{sc}$, $V_{oc}$ and Fill Factor and their standard deviations. Values in parentheses correspond to parameters of champion devices.



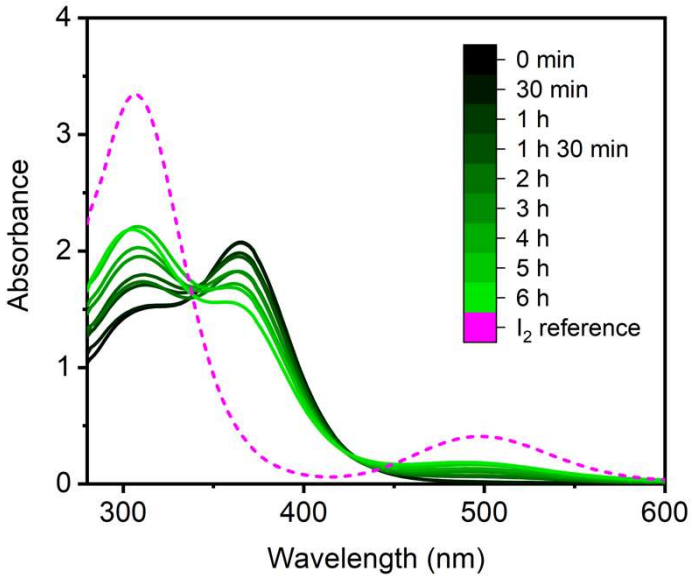

**Supplementary Figure 10.** Contour graphs representing $(PEA)_{0.2}(FA)_{0.8}SnI_3$ normalised absorbance (Abs(t)/Abs(0)) as a function of time and wavelength in films made with **a.** purified $SnI_2$, **b.** control $SnI_2$ and **c.** control $SnI_2$ + 2 mol% $SnI_4$.



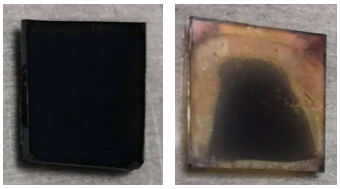

**Supplementary Figure 11.** Downfield proton nuclear magnetic resonance ($^1$H-NMR) spectra of DMSO-$d_6$, FAI, PEAI, fresh $(PEA)_{0.2}(FA)_{0.8}SnI_3$ and $(PEA)_{0.2}(FA)_{0.8}SnI_3$ aged for 24h in ambient air. Peaks in FAI ad PEAI spectra are assigned to protons in their respective molecules (see inset). The observed increase in multiplicity in degraded perovskite peaks assigned to FAI is attributed to the inhibition of the dynamic proton exchange between water and $FA^+$ upon $H_2O$ protonation.[6] This is attributed to the presence of $SnI_4$ and its reaction with $H_2O$ to form HI.



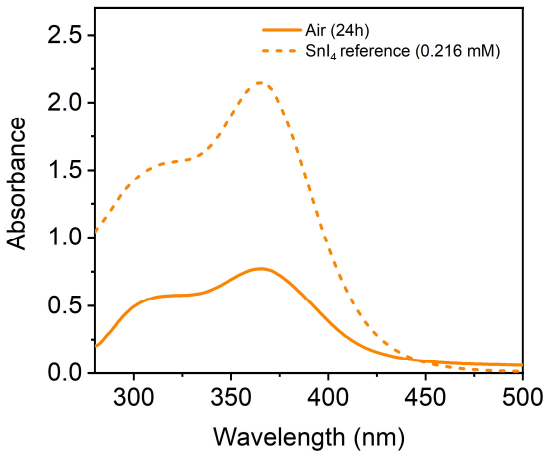

**Supplementary Figure 12. a.** Image of a vial filled with degassed deionized water after the addition of $SnI_4$. The white precipitate at the bottom corresponds to the formation of $SnO_2$ via Reaction 3 in the main paper. This experiment was carried out under inert $N_2$ atmosphere to rule out the involvement of $O_2$ in the reaction. **b.** pH test of deionized water vial before and after $SnI_4$ addition under $N_2$ atmosphere. The acidification of water upon $SnI_4$ addition is indicative of the formation of HI via hydrolysis (Reaction 3). **c.** Image of the $SnI_4$-treated vial after 4h exposure to ambient air. The change in colour from transparent to yellow/light brown indicates the presence of $I_3^-$ species. **d.** UV-Visible absorbance spectra of water before $SnI_4$ addition (blank), after $SnI_4$ addition/before air exposure and after $SnI_4$ addition/after 4h air exposure. The feature at ~ 250 nm is assigned to UV absorption by $SnO_2$ crystals (formed via Reaction 3). After air exposure, HI in solution is oxidized to $I_2$, which combines with remaining $I^-$ anions to give $I_3^-$ (peaks at ~285 and ~350 nm).



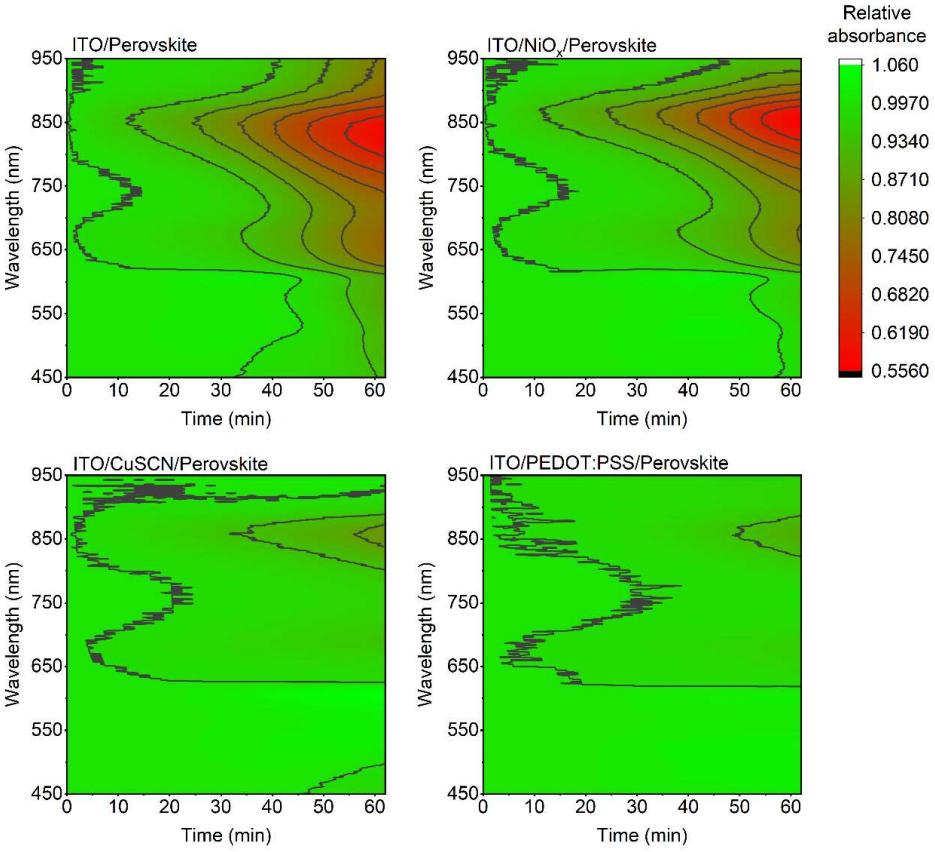

**Supplementary Figure 13.** Absorbance time evolution of a $SnI_4$ reference solution in toluene left in air for 6 hours and spectrum of an $I_2$ reference solution in toluene. The decrease of the absorption band at ~360 nm, the rise of spectral features at ~300 nm and ~500 nm and a colour change from orange to purple confirm the evolution of $SnI_4$ to $I_2$ in solution. Spectral changes over time are detected after only 30 min of ambient air exposure, suggesting the degradation of $SnI_4$ to $I_2$ is a relatively fast process.



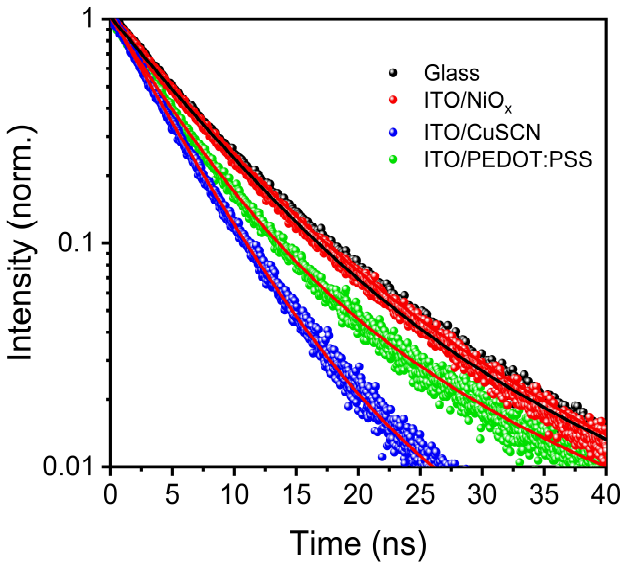
**Supplementary Figure 14.** Images of $(PEA)_{0.2}(FA)_{0.8}SnI_3$ perovskite thin films made with purified $SnI_2$ before degradation (left) and after being exposed to $I_2$ vapours in a $N_2$-filled glovebox for 3 minutes (right).



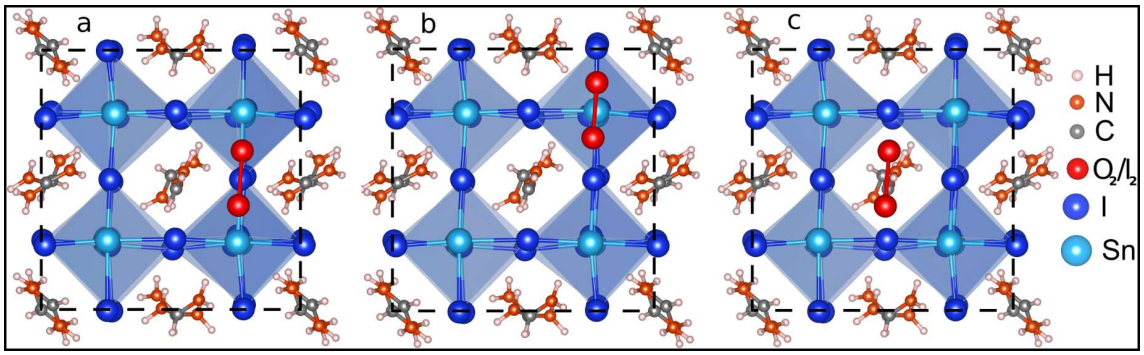

**Supplementary Figure 15.** UV-Visible spectrum of the degradation products extracted in toluene from a PMMA-free $(PEA)_{0.2}(FA)_{0.8}SnI_3$ thin film aged in ambient air for 24 h. The spectrum fully matches that of the $SnI_4$ reference solution (dashed line) and no features corresponding to $I_2$ are detected.



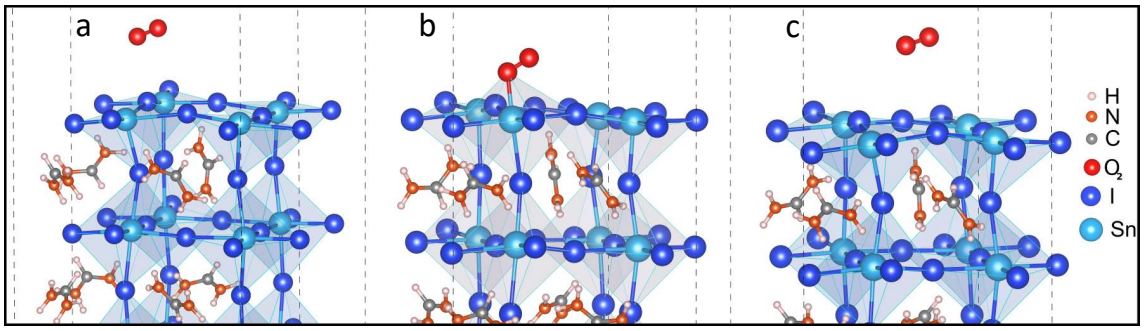

**Supplementary Figure 16.** Contour graphs showing the absorbance decay of $(PEA)_{0.2}(FA)_{0.8}SnI_3$ perovskite deposited on ITO and ITO/HTM substrates upon 1-hour exposure to ambient conditions (23ºC, 38% RH).



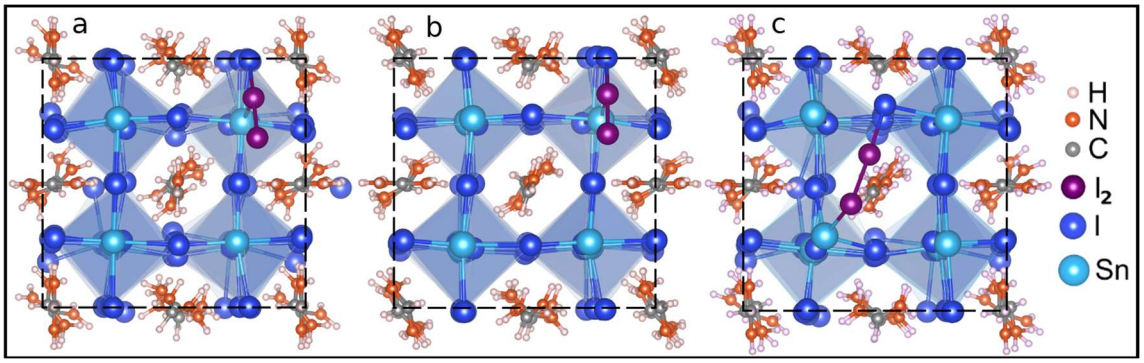

**Supplementary Figure 17**. Time-resolved PL decays of $(PEA)_{0.2}(FA)_{0.8}SnI_3$ films deposited on glass and ITO/HTM substrates acquired at 875 nm with 635 nm excitation and their biexponential fitting curves. Average $\tau_f$ values are 7.38 ns (glass/Perovskite), 7.31 ns (ITO/$NiO_x$/Perovskite), 4.71 ns (ITO/CuSCN/Perovskite) and 5.79 ns (ITO/PEDOT:PSS/Perovskite).



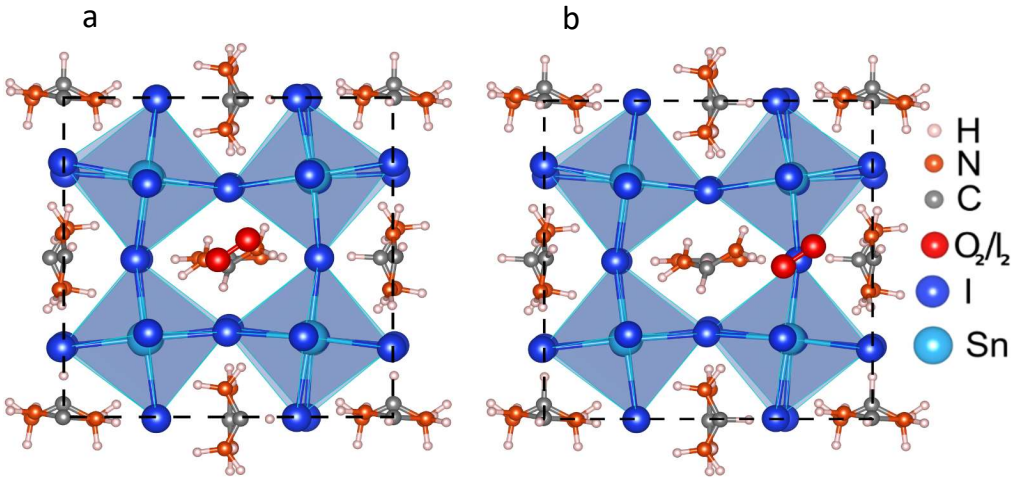

**Supplementary Figure 18**. Top view of the initial configurations of $O_2$ or $I_2$ molecules (red) on the (001) $FASnI_3$ surface with $SnI_2$ termination considered in this study. **a**. On top of the I atom, **b**. on top of the Sn and **c.** on the of the FA molecule of the $FASnI_3$ slab.



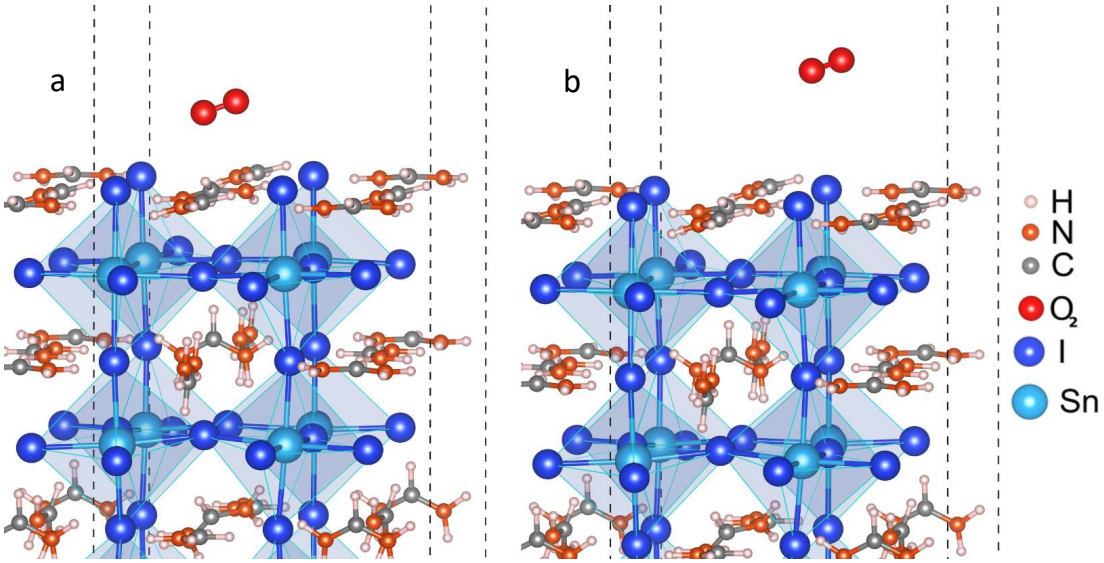

**Supplementary Figure 19**. Side view of the final configurations of $O_2$ molecule (red) on the (001) $FASnI_3$ surface with $SnI_2$ termination after relaxation starting **a**. on top of the I atom, **b**. on top of the Sn and **c**. on the of the FA molecule of the $FASnI_3$ slab.



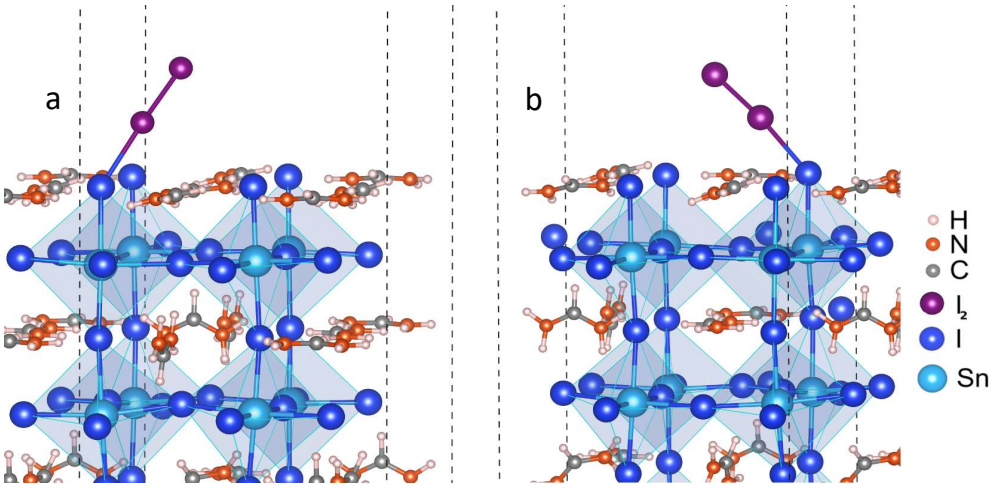

**Supplementary Figure 20**. Top view of the final configurations of $I_2$ molecule (red) on the (001) $FASnI_3$ surface with $SnI_2$ termination after relaxation starting **a**. on top of the I atom, **b**. on top of the Sn, and **c**. on the of the FA molecule of the $FASnI_3$ slab.




**Supplementary Figure 21**. Top view of the initial configurations of $O_2$ or $I_2$ molecules (red) on the (001) $FASnI_3$ surface with FAI termination considered in this study. **a**. On top of the FA molecule of the $FASnI_3$ slab. **b**. On top of the iodine atom of the $FASnI_3$ slab.




**Supplementary Figure 22.** Side view of the final configurations of $O_2$ molecule (red) on the (001) $FASnI_3$ surface with FAI termination after relaxation starting **a**. on top of the FA molecule or **b**. on top of the iodine atom of the $FASnI_3$ slab.




**Supplementary Figure 23.** Side view of the final configurations of $I_2$ molecule (purple colour) on the (001) $FASnI_3$ surface with FAI termination after relaxation starting **a**. on top of the FA molecule or **b**. on top of the iodine atom of the $FASnI_3$ slab.

## Supplementary References


1. Kubicki, D. J. *et al.* Local Structure and Dynamics in Methylammonium, Formamidinium, and Cesium Tin(II) Mixed-Halide Perovskites from $^{119}$Sn Solid-State NMR. *J. Am. Chem. Soc.* **142**, 7813–7826 (2020).

2. Leijtens, T., Prasanna, R., Gold-Parker, A., Toney, M. F. & McGehee, M. D. Mechanism of Tin Oxidation and Stabilization by Lead Substitution in Tin Halide Perovskites. *ACS Energy Lett.* **2**, 2159–2165 (2017).

3. Stoumpos, C. C., Malliakas, C. D. & Kanatzidis, M. G. Semiconducting Tin and Lead Iodide Perovskites with Organic Cations: Phase Transitions, High Mobilities, and Near-Infrared Photoluminescent Properties. *Inorg. Chem.* **52**, 9019–38 (2013).

4. Liao, Y. *et al.* Highly Oriented Low-Dimensional Tin Halide Perovskites with Enhanced Stability and Photovoltaic Performance. *J. Am. Chem. Soc.* **139**, 6693–6699 (2017).

5. Rath, T. *et al.* Photovoltaic properties of a triple cation methylammonium/formamidinium/phenylethylammonium tin iodide perovskite. *J. Mater. Chem. A* **7**, 9523–9529 (2019).

6. Van Gompel, W. T. M. *et al.* Degradation of the Formamidinium Cation and the Quantification of the Formamidinium−Methylammonium Ratio in Lead Iodide Hybrid Perovskites by Nuclear Magnetic Resonance Spectroscopy. *J. Phys. Chem. C* **122**, 4117–4124 (2018).